COBEM 2023 27TH INTERNATIONAL CONGRESS OF MECHANICAL ENGENEERING

ABCM Brazilian Society of Mechanical Sciences and Engineering
27th ABCM International Congress of Mechanical Engineering
December 04-08, 2023, Florianópolis-SC, Brazil

# ON THE EVALUATION OF NATURAL FREQUENCIES AND MODE SHAPES OF BEAMS UNDER TENSILE AXIAL LOADING

**Kevin Mauricio Menon Ribeiro**
Postgraduate Programme of Mechanical Engineering, Federal University of Paraná (UFPR) Av. Cel. Francisco H. dos Santos, 100 – Jardim das Américas, Curitiba – 81530-900 – Paraná, Brazil
eng.kevin.mmr@gmail.com
**Gabriel Ruggiero do Amaral**
Institute of Technology for Development – Lactec, Mechanical Testing Laboratory BR-116, km 98, 8813 – Jardim das Américas, Curitiba – 80.210-132 – Paraná, Brazil
gabriel.amaral@lactec.org.br
**José Manoel Balthazar**
Dept. of Mechanical Engineering, Engineering School, São Paulo State University (UNESP) – Bauru Av. Luís Edmundo Carrijo Coube, 14-01 – Vargem Limpa, Bauru – 17.033-360, São Paulo, Brazil
manoel.balthazar@unesp.br
**Alexandre de Macêdo Wahrhaftig**
Dept. of Construction and Structures, Polytechnic School, Federal University of Bahia (UFBA) Rua Aristides Novís, 02, 5th floor – Federação, Salvador – 40.210-910, Bahia, Brazil
alixa@ufba.br
**Eduardo Márcio de Oliveira Lopes**
Postgraduate Programme of Mechanical Engineering, Federal University of Paraná (UFPR) Av. Cel. Francisco H. dos Santos, 100 – Jardim das Américas, Curitiba – 81530-900 – Paraná, Brazil
eduardo_lopes@ufpr.br

***Abstract.*** *The accurate prediction of lateral vibration in beams subjected to axial loads is of great practical interest due to its wide use in describing the dynamic behavior of structures in the field of civil, mechanical, and aerospace engineering. Analytical solutions are classical mathematical procedures. Traditionally, the path taken in analytical solutions starts by admitting an acceptable kinematic hypothesis for a given problem, so that ultimately a closed mathematical equation can be obtained. Sometimes the problem can be implemented and solved numerically. A practical example of its application can be found in problems involving overhead transmission cables, for which the corresponding Euler-Bernoulli beam model is widely used. Although the analytical formulation for calculating natural frequencies and mode shapes for beams under tensile loading is well known and developed, it is worth noting that in certain applications, such as in the case of overhead cables, the results obtained may exhibit numerical instabilities for some boundary conditions. In the vast majority of studies, the mode shapes are described in terms of trigonometric and hyperbolic functions, despite the fact that hyperbolic functions tend to grow rapidly to infinity as their argument increases, which can cause numerical errors, especially in the vicinity of their supports. On the other hand, numerical simulations indicate that more accurate and reliable solutions can be obtained when the analytical solution is expressed by a linear combination of trigonometric and exponential terms. In this context, the present work aims to compare the two aforementioned ways of describing the analytical solution for calculating natural frequencies and their respective mode shapes of vibration with respect to overhead transmission line cables. In this effort, solutions are developed for two classical boundary conditions (fixed-fixed and fixed-simply supported) and one non-classical boundary condition (simply supported with torsional springs). Numerical simulations are carried out in the MATLAB environment. A significant gain is observed in the use of the presented formulation, especially in terms of a more accurate prediction of mode shapes for the type of structure under consideration.*

***Keywords:*** *analytical solution, axial loading, Euler-Bernoulli beam, mode shapes, overhead cables*

## 1. INTRODUCTION

Understanding the lateral vibration in beams under axial loading plays an important role in many engineering applications, including the design of overhead transmission cables, which is the focus of the present work. As a result, this phenomenon is extensively discussed in classical vibration theory references. However, the majority of these references consider the problem only in the context of simply supported beams, for which the natural frequencies can be computed analytically using closed-form solutions, and the modal shapes are described by pure sine functions.

In past decades, many researchers have made considerable efforts to develop solutions for calculating natural frequencies and mode shapes as design tools for the type of structure in question. Shaker (1975) studied the effect of compressive

axial loads on mode shapes and natural frequencies. Subsequently, Bokaian (1990) developed analytical solutions for calculating natural frequencies and mode shapes for tensile and compressed beams, under various classical boundary conditions. Maurizi and Belles (1991) derived the characteristic equation for calculating natural frequencies of compressed beams - under non-classical boundary conditions - including translational and rotational springs at the ends. Liu *et al.* (1996) developed the characteristic equation and mode shapes expression for free-free tensile beams in more detail. More recent works - such as those by Ceballos and Prato (2008), Foti *et al.* (2021), and Geuzaine *et al.* (2021) - present solutions related to mode shapes and natural frequencies for tensile beams subjected to the effect of torsional springs at the ends, with the aim of determining structural parameters from experimental tests.

Although the analytical formulation available in the literature on the subject is well known and developed, it has been observed through computational simulations that in certain applications, such as overhead transmission cables, the results can exhibit numerical instabilities for some boundary conditions of concern. That should be addressed, as pointed out below.

In general, the mode shapes found in the literature for Euler-Bernoulli beam problems are described in terms of hyperbolic and trigonometric functions. However, authors such as Tang (2003), Gonçalves *et al.* (2007), and Mazilu (2022) have observed that describing the vibration modes using hyperbolic functions can sometimes lead to numerically unstable modes. The cause of numerical instability is often related to floating-point calculations, particularly when computing the difference between two very large numbers. Floating-point calculations can result in a zero value instead of returning a small but significant number.

Nevertheless, numerical simulations demonstrate that more accurate solutions for the mode shapes of Euler-Bernoulli beams under axial loading are obtained when using a linear combination of trigonometric and exponential terms, as described in works by Franklin (1989), Main and Jones (2007), and Geuzaine *et al.* (2021). However, further development of this type of solution is still needed for different boundary conditions, the results of which can be used as a design tool in applications involving overhead transmission cables and other similar structures.

In this context, the present study aims to compare the two aforementioned ways of describing the analytical solution for calculating natural frequencies and mode shapes under classical and non-classical boundary conditions. These conditions may be encountered in real-life and laboratory bench situations, particularly in problems involving overhead transmission cables.

## 2. MATHEMATICAL DEVELOPMENT

The differential equation of motion for the free vibration of Euler-Bernoulli beam under tensile axial load is given by (Clough and Penzien, 1975):

$$EI\frac{\partial^4 y(x,t)}{\partial x^4} - T\frac{\partial^2 y(x,t)}{\partial x^2} + \rho A\frac{\partial^2 y(x,t)}{\partial t^2} = 0, \tag{1}$$

where $EI$ (Nm$^2$) is the flexural stiffness, $T$ (N) is the axial tension force, $\rho A$ (kg/m) is the mass per unit length, and $y(x,t)$ (m) is the lateral deflection of the beam in axial coordinate $x\ (m)$ at time $t$ (s).

Equation (1) can be solved using the method of separation of variables. Therefore, the lateral deflection $y(x,t)$ can be described as a function of two variables - a spatial variable $Y(x)$ and a temporal variable $G(t)$ - such that,

$$y(x,t) = Y(x)G(t), \tag{2}$$

whose expression allows rewriting Eq. (1) as follows:

$$-\frac{EI}{\rho A}\frac{1}{Y\left(x\right)}\frac{\partial^4 Y\left(x\right)}{\partial x^4} + \frac{T}{\rho A}\frac{1}{Y\left(x\right)}\frac{\partial^2 Y\left(x\right)}{\partial x^2} = \frac{1}{G(t)}\frac{\partial^2 G\left(t\right)}{\partial t^2} = -\omega^2. \tag{3}$$

Equation (3) allows dividing the problem into two parts, namely: a temporal problem and a spatial problem, represented by Eqs. (4) and (5), respectively, as follows:

$$\frac{d^2 G\left(t\right)}{dt^2} + \omega^2 G\left(t\right) = 0; \tag{4}$$

$$EI\frac{d^4 Y\left(x\right)}{dx^4} - T\frac{d^2 Y\left(x\right)}{dx^2} - \rho A\omega^2 Y\left(x\right) = 0. \tag{5}$$

The temporal problem has a harmonic solution of the following form:

$$G(t) = G_{os} sen\left(\omega t\right) + G_{oc}\cos\left(\omega t\right), \tag{6}$$

where $G_{os}$ and $G_{oc}$ are arbitrary constants to be determined by the initial conditions of the problem. On the other hand, the spatial problem defines an eigenvalue problem from which the natural frequencies $\omega_{n_j}$ and mode shapes $Y_{n_j}\left(x\right)$ are evaluated, as discussed in the following lines.

Introducing the dimensionless coordinate $\bar{x} = x/L$ into Eq. (5), where $L$ is the length of the beam such that $0 \leq \bar{x} \leq 1$, it yields:

$$\frac{d^4Y(\bar{x})}{d\bar{x}^4} - \frac{TL^2}{EI}\frac{d^2Y(\bar{x})}{d\bar{x}^2} - \frac{\rho A\omega^2 L^4}{EI}Y(\bar{x}) = 0, \tag{7}$$

also assuming that the solution of Eq. (7) has the form, $Y(\bar{x}) = Ce^{s\bar{x}}$, it follows that:

$$\left(s^4 - \frac{TL^2}{EI}s^2 - \frac{\rho A\omega^2 L^4}{EI}\right) = 0. \tag{8}$$

Equation 8 is quadratic in $s^2$ and hence can be easily solved. There are four roots, two of which are pure real roots and two of which are pure imaginary roots, in the following form:

$$s_1 = \pm M \quad s_2 = \pm iN \ , \tag{9}$$

where $M$ and $N$ are given by

$$\begin{aligned} M &= L\left\{(T/2EI) + \left[(T/2EI)^2 + (\rho A/EI)\,\omega^2\right]^{1/2}\right\}^{1/2} = \left(U + \sqrt{U^2+\Omega^4}\right)^{1/2} \\ N &= L\left\{-(T/2EI) + \left[(T/2EI)^2 + (\rho A/EI)\,\omega^2\right]^{1/2}\right\}^{1/2} = \left(-U + \sqrt{U^2+\Omega^4}\right)^{1/2}, \end{aligned} \tag{10}$$

and the dimensionless variables for flexural stiffness $\beta$, axial load $U$, and frequency $\Omega^4$ are defined, respectively, as

$$\beta = \frac{EI}{TL^2}, \quad U = \frac{1}{2\beta}, \quad \Omega^4 = \frac{\rho A\omega^2 L^4}{EI}. \tag{11}$$

The solution of the spatial problem - posed by (7) - is commonly provided in textbooks as,

$$Y(\bar{x} = x/L) = C_1 senhM\bar{x} + C_2 coshM\bar{x} + C_3 senN\bar{x} + C_4 cosN\bar{x}, \tag{12}$$

where the trigonometric terms represent propagating waves, and the hyperbolic terms represent evanescent waves. $C_1$, $C_2$, $C_3$, and $C_4$ are integration constants that need to be determined by imposing the boundary conditions.

Bokaian (1990) provides the frequency equations and integration constants for various classical boundary conditions based on Eq. (12). However, it is worth noting that the use of trigonometric and hyperbolic functions to express such a solution can sometimes lead to numerical instabilities. This instability arises due to the rapid growth of hyperbolic sine and cosine terms to infinity, while the numerical difference between them remains small. For this reason, authors such as Franklin (1989), Main and Jones (2007), and Geuzaine *et al.* (2021) emphasize that it is preferable to express the solution through a linear combination of trigonometric and exponential terms as,

$$Y(\bar{x} = x/L) = R_1 e^{-M\bar{x}} + R_2 e^{-M(1-\bar{x})} + R_3 senN\bar{x} + R_4 \cos N\bar{x}. \tag{13}$$

where $R_1$, $R_2$, $R_3$, and $R_4$ are the new integration constants, which must be determined by imposing the boundary conditions, as will be shown in the next sections.

### 2.1 Simply Supported Beam

The simply supported condition - whose boundary conditions are expressed by $Y(0) = 0$, $d^2Y(0)/dx^2 = 0, Y(L) = 0$, and $d^2Y(L)/dx^2 = 0$ - is the only one that has an analytical solution in closed form. Therefore, the natural frequencies and mode shapes can, respectively, be calculated using the following expressions:

$$\omega_{n_j} = \frac{\pi^2}{L^2}\sqrt{\frac{EI}{\rho A}}\left(j^4 + \frac{j^4 TL^2}{\pi^2 EI}\right)^{1/2} \tag{14}$$

$$Y_{n_j}(x) = \sin\left(\frac{j\pi x}{L}\right), \tag{15}$$

where $j = 1, 2, 3, ...$

### 2.2 Clamped – Clamped Beam

Consider now the case of a clamped-clamped beam, with boundary conditions $Y(0) = 0$, $dY(0)/dx = 0$, $Y(L) = 0$, and $dY(L)/dx = 0$. The expression for the j$^{th}$ mode shape is given by (Bokaian, 1990):

$$Y_{n_j}(x) = \sinh\left(\frac{Mx}{L}\right) + \left[\frac{M\sin N - N\sinh M}{N\left(\cosh M - \cos N\right)}\right]\cosh\left(\frac{Mx}{L}\right) + ... \\ ... - \left(\frac{M}{N}\right)\sin\left(\frac{Nx}{L}\right) - \left[\frac{M\sin N - N\sinh M}{N\left(\cosh M - \cos N\right)}\right]\cos\left(\frac{Nx}{L}\right), \tag{16}$$

where $M$ and $N$ can be obtained by solving the following frequency equation:

$$\Omega - Usinh\left(M\right)\sin\left(N\right) - \Omega\cosh\left(N\right)\cos\left(N\right) = 0, \tag{17}$$

along with the use of the relationships provided by Eqs. (10) and (11).

The revised expression of the mode shapes for the clamped-clamped condition - now written in terms of exponential and trigonometric functions - is obtained by applying the boundary conditions in the solution given by Eq. (13), whose resulting expression is given by

$$Y_{n_j}\left(x\right) = \left(\frac{N}{M}\right)\exp\left(\frac{-Mx}{L}\right) + \left(\frac{N}{M}\cos N - senN\right)\exp\left[\frac{M\left(L-x\right)}{L}\right] + ... \\ ... + sen\left(\frac{Nx}{L}\right) - \left(\frac{N}{M}\right)\cos\left(\frac{Nx}{L}\right), \tag{18}$$

where $M$ and $N$ are now obtained by solving the following frequency equation:

$$(N^2 - M^2)sin\left(N\right) + 2MN\cos\left(N\right) = 0. \tag{19}$$

It is worth noting that Eqs. (17) and (19), as well as the frequency equations for the other boundary conditions, take the form of a transcendental equation, which has an infinite number of roots. Therefore, these roots must generally be determined numerically.

### 2.3 Clamped - Supported Beam

Addressing the case of a clamped-supported beam, for which the boundary conditions are $Y(0) = 0$, $dY(0)/dx = 0$, $Y(L) = 0$, and $d^2Y(L)/dx^2 = 0$, the expression for the j$^{th}$ mode shape is given by (Bokaian, 1990):

$$Y_{n_j}\left(x\right) = senh\left(\frac{Mx}{L}\right) - \tanh M\cosh\left(\frac{Mx}{L}\right) - \frac{M}{N}sen\left(\frac{Nx}{L}\right) + \frac{M}{N}\tan N\cos\left(\frac{Nx}{L}\right), \tag{20}$$

where $M$ and $N$ can be obtained by solving the following frequency equation:

$$M\cosh\left(M\right)\sin\left(N\right) - N\sinh\left(M\right)\cos\left(N\right) = 0. \tag{21}$$

The revised mode shape function, described now in terms of exponential and trigonometric terms, arising from the solution provided by Eq. (13), is expressed as follows:

$$Y_{n_j}\left(x\right) = \left(\frac{N}{M}\right)\exp\left(\frac{-Mx}{L}\right) + \left(\frac{N}{M}\cos N - senN\right)\exp\left[\frac{M\left(L-x\right)}{L}\right] + ... \\ ... + sen\left(\frac{Nx}{L}\right) - \left(\frac{N}{M}\right)\cos\left(\frac{Nx}{L}\right), \tag{22}$$

where now $M$ and $N$ are obtained by solving the following frequency equation:

$$(M^2 + N^2)\left[N\cos\left(N\right) - M\sin\left(N\right)\right] = 0. \tag{23}$$

### 2.4 Supported Beam with Torsional Springs

Despite the extreme importance of developing solutions for classical boundary conditions, it is known that in real situations, end constraints are rarely infinitely rigid in rotation. Thus, it is crucial to analyze boundary conditions that consider the effect of torsional springs at their ends, as illustrated in Fig. 1

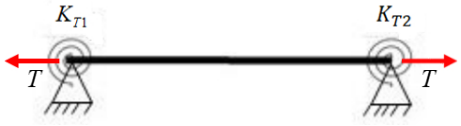


Figure 1. Supported beam under tensile load with torsional springs

The boundary conditions for the structural system under consideration are as follows: at $x = 0$,

$$Y\left(x=0\right)=0, \tag{24}$$

$$K_{T1}\frac{\partial Y(x=0)}{\partial x}=EI\frac{\partial^2 Y(x=0)}{\partial x^2}, \tag{25}$$

and at $x = L$,

$$Y\left(x=L\right)=0, \tag{26}$$

$$K_{T2}\frac{\partial Y(x=L)}{\partial x}=-EI\frac{\partial^2 Y(x=L)}{\partial x^2}, \tag{27}$$

where $K_{T1}$ and $K_{T2}$ are torsional spring constants.

The application of these boundary conditions to Eq. (13) results in the following system of algebraic equations:

$$\begin{array}{l} R_1+\left(\exp(-M)\right)R_2+R_4=0,\quad \left(\exp(-M)\right)R_1+R_2+\left(sinN\right)R_3+\left(\cos N\right)R_4=0,\\ -\left(R_{T1}M^2+M\right)R_1+\left[\exp(-M)(M-R_{T1}M^2)\right]R_2+NR_3+R_{T1}N^2R_4=0,\\ \left[\exp(-M)(R_{T2}M^2-M)\right]R_1+\left(R_{T2}M^2+M\right)R_2+\left(N\cos N-R_{T2}N^2sinN\right)R_3+...\\ ...-\left(NsinN+R_{T2}N^2\cos N\right)R_4=0, \end{array} \tag{28}$$

where $R_{T1} = EI/K_{T1}L$ and $R_{T1} = EI/K_{T1}L$ are the dimensionless constants of the torsional springs.

For the specific case of applications in overhead transmission cables, where the structural system is long, slender, and subjected to a high axial force, it is valid to consider that $\beta \ll 1$, which leads to the observation that $e^{-M} \to 0$, and therefore its effect can be neglected. Therefore, Eq. (28) can be simplified as follows:

$$\begin{array}{l} R_1+R_4=0,\quad R_2+\left(sinN\right)R_3+\left(\cos N\right)R_4=0,\\ -\left(R_{T1}M^2+M\right)R_1+NR_3+R_{T1}N^2R_4=0,\\ \left(R_{T2}M^2+M\right)R_2+\left(N\cos N-R_{T2}N^2sinN\right)R_3-\left(Nsin'N+R_{T2}N^2\cos N\right)R_4=0. \end{array} \tag{29}$$

For the solution to be nontrivial, the determinant of the coefficient matrix in Eq. (29) must be zero, resulting in the following frequency equation:

$$A_C\sin N+B_C\cos N=0, \tag{30}$$

where

$$\begin{array}{l} A_C=N^2(1-R_{T1}R_{T2}N^2)-M^2(MR_{T1}+MR_{T2}+M^2R_{T1}R_{T2}+1)...\\ ...-MN^2\left(R_{T1}+R_{T2}\right)-2R_{T1}R_{T2}M^2N^2,\\ B_C=N^3(R_{T1}+R_{T2})+M^2N\left(R_{T1}+R_{T2}\right)+2MN. \end{array} \tag{31}$$

By solving the homogeneous system of algebraic equations for the unknowns $R_1$, $R_2$, $R_3$, and $R_4$, the following expression for the modal shape is obtained:

$$\begin{array}{l} Y_{n_j}\left(x\right)=\sin\left(\dfrac{Nx}{L}\right)-\sin\left(N\right)\exp\left[-M\left(\dfrac{L-x}{x}\right)\right]+...\\ ...+\beta_n\left\{\exp\left(-Mx\right)+\cos\left(N\right)\exp\left[-M\left(\dfrac{L-x}{x}\right)\right]-\cos\left(\dfrac{Nx}{L}\right)\right\}, \end{array} \tag{32}$$

where

$$\beta_n=\frac{N}{R_{T1}N^2+R_{T1}M^2+M}. \tag{33}$$

In order to adapt the above formulation to a system with classical boundary conditions, the dimensionless constants of the torsional springs must be modified, as shown in Tab. 1.

Table 1. Limit values of the dimensionless parameter of torsional springs

| **Boundary Condition** | $\mathbf{R_{T1}}$ | $\mathbf{R_{T2}}$ |
|---|---|---|
| Simply supported | $R_{T1} \to \infty$ | $R_{T2} \to \infty$ |
| Clamped – clamped | $R_{T1} \to 0$ | $R_{T1} \to 0$ |
| Clamped – supported | $R_{T1} \to 0$ | $R_{T2} \to \infty$ |

## 3. FEM SOLUTION

To validate the analytical solution presented in the previous section, a numerical simulation using FEM was carried out. This is basically an eigenvalues problem, which can be expressed as

$$\left(\mathbf{K} - \omega^2 \mathbf{M}\right) \phi = 0 \tag{34}$$

where $\mathbf{M}$ is the mass matrix of the structure, and $\mathbf{K}$ is the corresponding stiffness matrix. In Eq. (34), $\omega^2$ are the eigenvalues and $\phi$ are the eigenvectors. In this case, the $n$ solutions for $\omega_i^2$ are real and positive, apart from being the squares of the natural frequencies of the system. The known matrices for the mass and stiffness of the four-degree-of-freedom linear planar beam finite elements are (Yang and Kuo, 1994):

$$\mathbf{M^e} = \frac{\rho A L_e}{420} \begin{bmatrix} 156 & 22L_e & 54 & -13L_e \\ 22L_e & 4L_e^2 & 13L_e & -3L_e^2 \\ 54 & 13L_e & 156 & -22L_e \\ -13L_e & -3L_e^2 & -22L_e & 4L_e^2 \end{bmatrix}, \tag{35}$$

and

$$\mathbf{K^e} = \mathbf{K_E^e} + \mathbf{K_T^e}, \tag{36}$$

where

$$\mathbf{K}_E^e = \frac{EI}{L_e^3} \begin{bmatrix} 12 & 6L_e & -12 & 6L_e \\ 6L_e & 4L_e^2 & -6L_e & 2L_e^2 \\ -12 & -6L_e & 12 & -6L_e \\ 6L_e & 2L_e^2 & -6L_e & 4L_e^2 \end{bmatrix} \quad \mathbf{K}_T^e = \frac{T}{30L_e} \begin{bmatrix} 36 & 3L_e & -36 & 3L_e \\ 3L_e & 4L_e^2 & -3L_e & -L_e^2 \\ -36 & -3L_e & 36 & -3L_e \\ 3L_e & -L_e^2 & -3L_e & 4L_e^2 \end{bmatrix} \tag{37}$$

and $L_e$ is the element length.

The FEM model is implemented in the MATLAB environment with 150 elements.

## 4. NUMERICAL SIMULATIONS

For the numerical simulations, an aluminum alloy conductor (CAL), used as an overhead cable in power lines, was considered with the following parameters: flexural stiffness $EI = 271.3$ Nm$^2$, mass per unit length $\rho A = 0.6870$ kg/m, span length $L = 30.2$ m, and tensile force $T = 13091$ N.

All the analytical solutions developed in section 2 were all implemented in the Matlab environment. In order to solve the transcendental frequency equations, the bisection method was applied using of the existing fzeros function in Matlab. Consequently, once the j$^{th}$ natural frequency $\omega_{n_j}$ is obtained, it is possible to calculate the corresponding j$^{th}$ mode shape $Y_{n_j}(x)$.

The following abbreviations are also used below: E – T denotes the solution described in exponential and trigonometric terms, while H – T refers to the solution described in hyperbolic and trigonometric terms.

### 4.1 Clamped - Clamped Condition

The first eight natural frequencies obtained from the frequency equations given by Eqs. (17), (19) and by the Eq. (30) with $R_{T1} \to 0$ and $R_{T2} \to 0$, as well as the natural frequencies obtained by the finite element method - for the clamped-clamped boundary condition - are shown in Tab. 2. Figures 2 and 4 show the $7^{th}$ and $8^{th}$ vibration mode shapes, respectively, obtained from the numerical simulations for the clamped-clamped condition.

Figures 3 and 5 provide an enlarged view of the numerical results, focusing on the regions surrounding the right and left ends of the structure. In addition, a zoomed-in view of the numerically unstable region is presented for the $7^{th}$ and $8^{th}$ modal shapes, considering the clamped-clamped boundary condition.

From the Figures 2, 3, 4, and 5, it is evident that the exponential and trigonometric-based solution demonstrates strong agreement with FEM results for the clamped-clamped condition. Moreover, this solution provides a more precise depiction, particularly in the boundary regions, when compared to the hyperbolic and trigonometric-based solution.

Table 2. Values of natural frequencies ($f_{n_j}$) in Hz for the clamped-clamped boundary condition

| **Natural frequencies $\mathbf{f_{n_j}}$** | $\mathbf{j=1}$ | $\mathbf{j=2}$ | $\mathbf{j=3}$ | $\mathbf{j=4}$ | $\mathbf{j=5}$ | $\mathbf{j=6}$ | $\mathbf{j=7}$ | $\mathbf{j=8}$ |
|---|---|---|---|---|---|---|---|---|
| Exponential and trigonometric terms$^{(1)}$ | 2.3065 | 4.6143 | 6.9249 | 9.2397 | 11.560 | 13.8872 | 16.2227 | 18.5679 |
| Hyperbolic and trigonometric Terms$^{(2)}$ | 2.3065 | 4.6143 | 6.9249 | 9.2397 | 11.560 | 13.8872 | 16.2227 | 18.5679 |
| Rotational springs$^{(3)}$ | 2.3065 | 4.6143 | 6.9249 | 9.2397 | 11.560 | 13.8872 | 16.2227 | 18.5679 |
| FEM | 2.3065 | 4.6144 | 6.9251 | 9.2399 | 11.5603 | 13.8876 | 16.2231 | 18.5683 |

$^{(1)}$ Eq. (17); $^{(2)}$ Eq. (19); $^{(3)}$ Eq. (30) with $R_{T1} \to 0$ and $R_{T2} \to 0$.

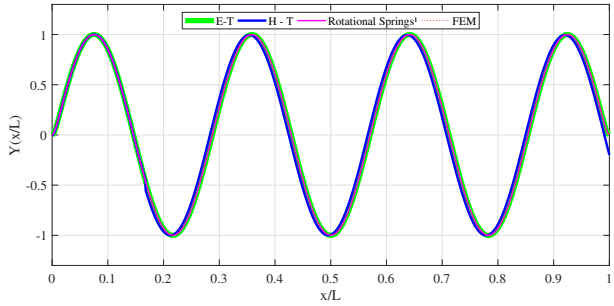


Figure 2. Clamped – clamped boundary condition – 7th mode shape.
$^{(1)}$ $R_{T1} \to 0$ and $R_{T2} \to 0$.

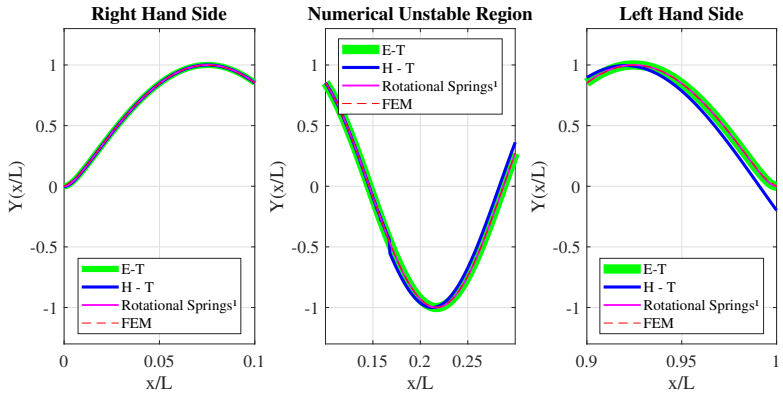


Figure 3. Zoomed-in view of the right and left-hand side ends – Clamped – clamped boundary condition – 7th mode shape.
$^{(1)}$ $R_{T1} \to 0$ and $R_{T2} \to 0$

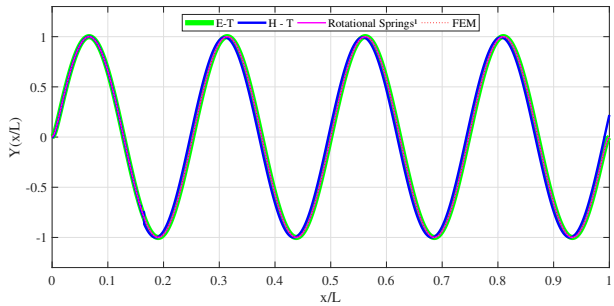


Figure 4. Clamped – clamped boundary condition – 8th mode shape.
$^{(1)}$ $R_{T1} \to 0$ and $R_{T2} \to 0$.

### 4.2 Clamped – Supported Condition

The first eight natural frequencies obtained from the frequency equations given by the Eqs. (21), (23) and by the Eq. (30) with $R_{T1} \to 0$ and $R_{T2} \to \infty$, as well as the natural frequencies obtained by the finite element method - for the clamped-clamped boundary condition - are shown in Tab. 3. Figures 6 and 8 show the $7^{th}$ and $8^{th}$ vibration mode shapes, respectively, obtained from the numerical simulations for the clamped-supported condition.

Figures 7 and 9 show an enlarged view of the numerical results, focusing on the regions around the right and left ends of the structure. These figures also provide a zoomed-in view of the numerically unstable region for the $7^{th}$ and $8^{th}$ modal shapes under the clamped-supported boundary condition.

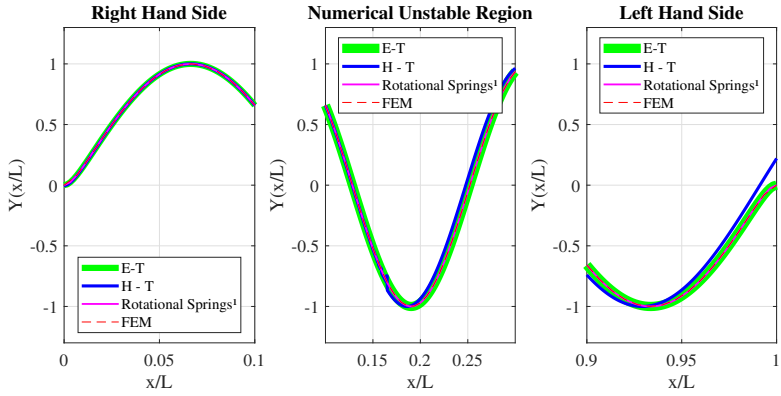


Figure 5. Zoomed-in view of the right and left-hand side ends – Clamped – clamped boundary condition – 8th mode shape.
(1) $R_{T1} \to 0$ and $R_{T2} \to 0$

Table 3. Values of natural frequencies ($f_{n_j}$) in Hz for the clamped-supported boundary condition

| **Natural frequencies $\mathbf{f_{n_j}}$** | $\mathbf{j=1}$ | $\mathbf{j=2}$ | $\mathbf{j=3}$ | $\mathbf{j=4}$ | $\mathbf{j=5}$ | $\mathbf{j=6}$ | $\mathbf{j=7}$ | $\mathbf{j=8}$ |
|---|---|---|---|---|---|---|---|---|
| Exponential and trigonometric terms(1) | 2.2960 | 4.5934 | 6.8936 | 9.1979 | 11.5077 | 13.8243 | 16.1492 | 18.4837 |
| Hyperbolic and trigonometric terms(2) | 2.2960 | 4.5934 | 6.8936 | 9.1979 | 11.5077 | 13.8243 | 16.1492 | 18.4837 |
| Rotational springs(3) | 2.2960 | 4.5934 | 6.8936 | 9.1979 | 11.5077 | 13.8243 | 16.1492 | 18.4837 |
| FEM | 2.2960 | 4.5935 | 6.8937 | 9.1980 | 11.5078 | 13.8245 | 16.1494 | 18.4840 |

(1) Eq. (23); (2) Eq. (21) (3) Eq. (30) with $R_{T1} \to 0$ and $R_{T2} \to \infty$.

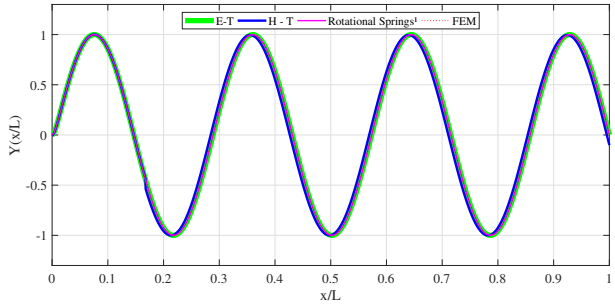


Figure 6. Clamped – supported boundary condition – 7th mode shape.
(1) $R_{T1} \to 0$ and $R_{T2} \to \infty$.

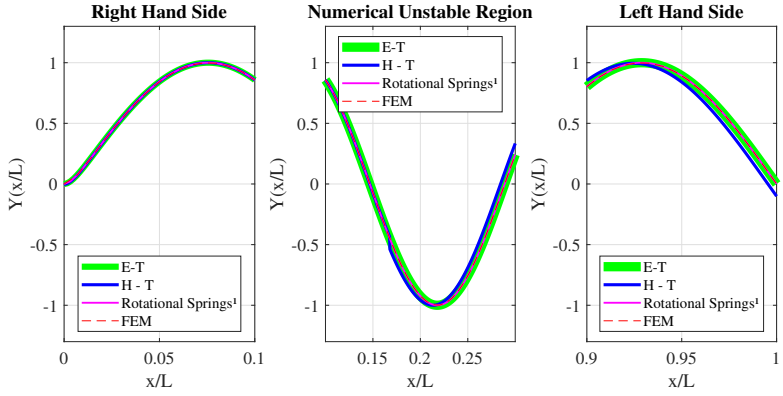


Figure 7. Zoomed-in view of the right and left-hand side ends – Clamped – supported boundary condition – 7th mode shape.
(1) $R_{T1} \to 0$ and $R_{T2} \to \infty$

The Figures 6, 7, 8, 9 clearly demonstrate the strong agreement between the exponential and trigonometric-based solution and the FEM results for the clamped-supported condition.

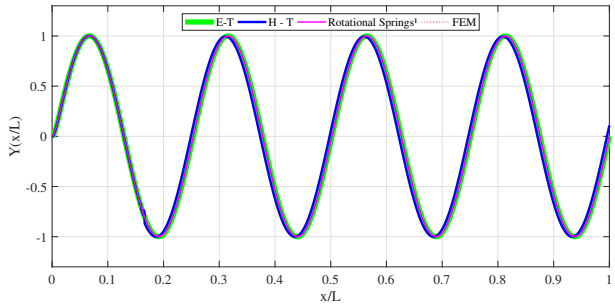


Figure 8. Clamped – supported boundary condition – 7th mode shape.
(1) $R_{T1} \to 0$ and $R_{T2} \to \infty$.

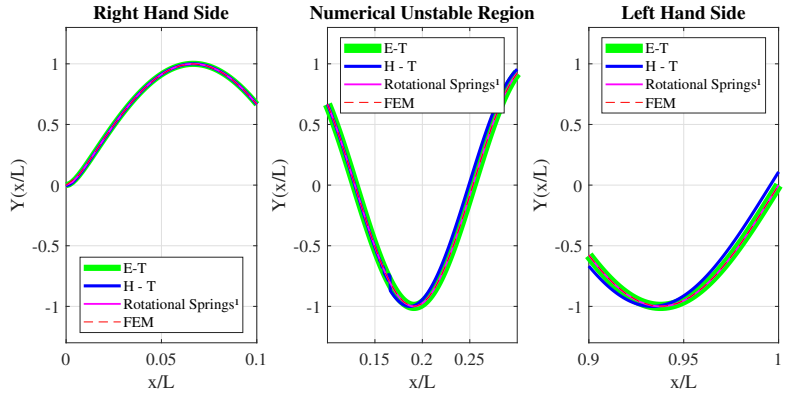


Figure 9. Zoomed-in view of the right and left-hand side ends – Clamped – supported boundary condition – 7th mode shape.
(1) $R_{T1} \to 0$ and $R_{T2} \to \infty$

## 5. CONCLUSIONS

There is a strong agreement between the results obtained through Finite Element Method (FEM) and those obtained from Eqs. (18), (22), and (32), where the solution is expressed in exponential and trigonometric terms for the corresponding boundary conditions. This fact confirms that the solution expressed in exponential and trigonometric terms gives a remarkably accurate prediction, especially near the ends of the structure. Therefore, the formulation presented here shows a significant improvement in the prediction of mode shapes for problems involving overhead cables of power lines.

Moreover, it is essential to emphasize that achieving a more accurate representation of mode shapes and natural frequencies will facilitate a more detailed characterization of Frequency Response Functions (FRFs) in future studies. These FRFs hold significant potential for material parameter identification in overhead cables, in which there are some typically unknown dynamic parameters, such as those related to damping. This identification process can be realized through comparative analysis with experimental data, aiming the better understanding of the cable's mechanical properties.

## 6. ACKNOWLEDGEMENTS

José M. Balthazar, Alexandre M. Wahrhaftig and Eduardo M. O. Lopes acknowledge the support of CNPq - National Council for Scientific and Technological Development for their scholarships.

## 7. REFERENCES

Bokaian, A., 1990. "Natural frequencies of beams under tensile axial loads". *Journal of Sound and Vibration*, Vol. 142, No. 3, pp. 481–498.

Ceballos, M.A. and Prato, C.A., 2008. "Determination of the axial force on stay cables accounting for their bending stiffness and rotational end restraints by free vibration tests". *Journal of Sound and Vibration*, Vol. 317, No. 1-2, pp. 127–141.

Clough, R. and Penzien, J., 1975. *Dynamics of Structures*. McGraw-Hill NY, USA.

Foti, F., Geuzaine, M. and Denoël, V., 2021. "On the identification of the axial force and bending stiffness of stay cables anchored to flexible supports". *Applied Mathematical Modelling*, Vol. 92, pp. 798–828.

Franklin, P.A., 1989. *Modal analysis of long systems: a transfer matrix approach*. Ph.D. thesis, Johns Hopkins University.

Geuzaine, M., Foti, F. and Denoël, V., 2021. "Minimal requirements for the vibration-based identification of the axial

force, the bending stiffness and the flexural boundary conditions in cables". *Journal of Sound and Vibration*, Vol. 511, p. 116326.

Gonçalves, P., Brennan, M. and Elliott, S., 2007. "Numerical evaluation of high-order modes of vibration in uniform Euler–Bernoulli beams". *Journal of Sound and Vibration*, Vol. 301, No. 3-5, pp. 1035–1039.

Liu, X., Ertekin, R. and Riggs, H., 1996. "Vibration of a free-free beam under tensile axial loads". *Journal of Sound and Vibration*, Vol. 190, No. 2, pp. 273–282.

Main, J.A. and Jones, N.P., 2007. "Vibration of tensioned beams with intermediate damper. i: Formulation, influence of damper location". *Journal of Engineering Mechanics*, Vol. 133, No. 4, pp. 369–378.

Maurizi, M. and Belles, P., 1991. "General equation of frequencies for vibrating uniform one-span beams under compressive axial loads". *Journal of Sound Vibration*, Vol. 145, No. 2, pp. 345–347.

Mazilu, T., 2022. "Numerically stable form of Green's function for a free-free uniform Timoshenko beam". *Mathematics*, Vol. 11, No. 1, p. 86.

Shaker, F.J., 1975. "Effect of axial load on mode shapes and frequencies of beams". Nasa technical note (nasa-tn-d-8109).

Tang, Y., 2003. "Numerical evaluation of uniform beam modes". *Journal of Engineering Mechanics*, Vol. 129, No. 12, pp. 1475–1477.

Yang, Y.B. and Kuo, S.R., 1994. *Theory & analysis of nonlinear framed structures*. Pearson Ed.

## 8. RESPONSIBILITY NOTICE

The authors are solely responsible for the printed material included in this paper.